Int. J. Rock Mech. Min. Sci. & Geomech. Abstr. Vol. 22, No. 5, pp. 291–302, 1985
Printed in Great Britain

0148-9062/85 $3.00 + 0.00
Pergamon Press Ltd

Gravitational Stresses in Long Symmetric Ridges and Valleys

W. Z. SAVAGE*
H. S. SWOLFS
P. S. POWERS

The effect of topography on near-surface, gravity-induced stresses has been analysed using an elastic solution similar to one originally given by Akhpatelov and co-workers. The topographic features considered here are isolated symmetric ridges and valleys, and explicit solutions are presented for these particular features. The main results are: (1) non-zero horizontal compressive stresses develop at and near ridge crests and decrease with increasing Poisson's ratio, and (2) horizontal tensile stresses develop under the valley, but decrease and become compressive with increasing Poisson's ratio. For both geometries, all stresses increase with depth and approach a standard state of stress. The magnitude of the topographically induced stresses is on the order of the characteristic stress $\rho \mathbf{g} b$, *where* b *is the height of the ridge or the depth of the valley.*

INTRODUCTION

Horizontal stresses measured in the near surface of the earth's crust, either by overcoring or hydrofracturing, are nearly always compressive and in excess of the vertical stress due to the weight of overburden [1–3]. Because these measured horizontal stresses are not always zero at the surface of the earth, they have been variably interpreted as being of tectonic, thermal, or residual origin (see [1] for further discussion). For the most part, except in regions of rugged topography [4], local topographic effects in areas of subdued relief were not thought to affect near-surface stresses. The recent work of McTigue and Mei [5], however, focuses attention on the fact that topography affects the gravitationally induced horizontal stresses even in areas of low, regional slope. Similar observations can be made from the work of Akhpatelov and others [see 6, pp. 166–167], which is considered in greater detail in this paper.

Because of mathematical difficulties, few exact solutions exist for gravitational stresses in elastic media with irregular boundaries. Baladi [7] and Perloff *et al.* [8] present an exact solution for gravitational stresses in a trapezoidal embankment. These solutions are obtained by the Kolosov–Muskhelishvili method of complex potentials for plane elasticity. A Schwarz–Christoffel transformation maps the trapezoidal embankments into a half plane. Unfortunately, the numerical scheme used to evaluate the integral for the mapping function does not account for branch cuts [5, 9]. Consequently, the solutions of Baladi [7] and Perloff *et al.* [8] may be in error. Silvestri and Tabib [10, 11] present exact solutions for stresses in finite elastic slopes using similar methods to those mentioned above. They include a solution for the interesting problem of gravity stresses in a vertical topographic step or wall.

Akhpatelov and Ter-Martirosyan [12], Ter-Martirosyan and Akhpatelov [13] and Ter-Martirosyan *et al.* [14] give exact solutions for gravitational stresses in elastic half-spaces with smooth curvilinear boundaries. Some of their results for gravitational stresses in symmetrical "hills" and "canyons" are illustrated in a review article by Tsytovich [6]. A different approach is taken by McTigue and Mei [5]; specifically, a perturbation method is used to obtain approximate analytical solutions for gravity stresses in elastic half spaces with curvilinear boundaries and small characteristic slopes.

Although the work of Akhpatelov and co-workers [12–14] is of considerable interest and importance, much of it is published in Russian journals of limited availability in the West. Moreover, in the available articles, critical mathematical steps involved in obtaining the closed-form solutions are omitted and too few examples are given to illustrate applications of the results. Because of the paucity of mathematical detail, it was necessary to rederive the solutions for gravity-induced stresses in isolated symmetric ridges and valleys. In what follows, the complete derivation for the solution of this important problem is given and a number of examples to illustrate the application of the results are presented. Comparisons will also be made with the results of the perturbation method of McTigue and Mei [5] for an isolated, symmetric ridge of small slope.

* All authors work at: U.S. Geological Survey, Box 25046, MS 966, Denver Federal Center, Denver, CO 80225, U.S.A.

SOLUTION FOR GRAVITATIONAL STRESSES IN A SYMMETRIC RIDGE OR VALLEY

Only a brief review of the Kolosov–Muskhelishvili method for solving plane elasto-static problems will be given here. Detailed treatments may be found in Muskhelishvili [15], Sokolnikoff [16] and Baladi [7].

For a plane elasto-static problem in orthogonal Cartesian co-ordinates (Fig. 1) where a constant body force, ρg, is directed along the vertical y-axis, the equations of equilibrium reduce to

$$\frac{\partial \sigma_x}{\partial x} + \frac{\partial \sigma_{yx}}{\partial y} = 0, \tag{1a}$$

$$\frac{\partial \sigma_{xy}}{\partial x} + \frac{\partial \sigma_y}{\partial y} - \rho g = 0, \tag{1b}$$

where ρ is the mass per unit volume, g is the gravitational acceleration, σ_x and σ_y are the normal components of stress and σ_{yx} and σ_{xy} are the shear components of stress all acting in the x- and y-directions, respectively. Because the resultant moment of body and surface forces over the body vanishes, σ_{xy} can be shown to be equal to σ_{yx} [16, pp. 41–42]. Tensile normal stresses are taken to be positive.

For the problem of interest, a long symmetric ridge or valley under gravity, it is assumed that strains acting in the direction of the axis of the ridge or valley vanish. Hence, a state of plane strain with three non-vanishing components of strain exists with two non-vanishing components of displacement acting in planes normal to the ridge or valley axis. These strains are functions of the displacements, and because the number of strain components exceeds the number of displacement components by one an additional relation between the strain components must be satisfied: namely, the equation of compatibility. By using Hooke's law for an isotropic medium [16] this equation is expressed in terms of stresses as,

$$\nabla^2(\sigma_x + \sigma_y) = 0. \tag{2}$$

Note also that under plane strain conditions Hooke's law requires that a third normal stress component, σ_z, will act parallel to the ridge or valley axis. It can be easily shown to be given by [16, p. 251]

$$\sigma_z = \mu(\sigma_x + \sigma_y), \tag{3}$$

where μ is Poisson's ratio. In addition, stresses at the surface of an elastic body must satisfy certain boundary conditions which in two dimensions can be expressed as

$$\overset{n}{T}_x = n_x\sigma_x + n_y\sigma_{xy}, \tag{4a}$$

$$\overset{n}{T}_y = n_x\sigma_{xy} + n_y\sigma_y, \tag{4b}$$

where $\overset{n}{T}_x$ and $\overset{n}{T}_y$ are the components of surface force per unit area (tractions) at a point on the boundary and n_x and n_y are the direction cosines of the normal n to the boundary at that point. Finally, if the stresses are related to the Airy stress function $U(x, y)$ by

$$\sigma_x = \frac{\partial^2 U(x,y)}{\partial y^2} + \frac{\mu}{1-\mu}\rho g y, \tag{5a}$$

$$\sigma_y = \frac{\partial^2 U(x,y)}{\partial x^2} + \rho g y, \tag{5b}$$

$$\sigma_{xy} = \frac{-\partial^2 U(x,y)}{\partial x \partial y}, \tag{5c}$$

the equilibrium equations (equations 1a and b) are satisfied identically. The terms $[\mu/1-\mu]\rho g y$ and $\rho g y$ are taken to represent a standard state of stress for a flat-lying horizontal region under gravity [18, p. 356]. Inserting equations (5a) and (b) in the compatibility equation (equation 2) it is found that $U(x, y)$ satisfies the biharmonic equation

$$\nabla^4 U(x,y) = \frac{\partial^4 U}{\partial x^4} + 2\frac{\partial^4 U}{\partial x^2 \partial y^2} + \frac{\partial^4 U}{\partial y^4} = 0. \tag{6}$$

Solutions to equation (6) yield general solutions for stresses and displacements which satisfy equilibrium (equations 1) and compatibility (equation 2). Specification of the stress function $U(x, y)$ to give stresses which satisfy particular boundary conditions (equations 4a and b) then result in complete solutions for stresses and displacements in gravitating elastic bodies under conditions of plane strain. A variety of methods can be used to find those solutions. Among the more powerful is that of Kolosov–Muskhelishvili. It can be shown [15, p. 110] that a general solution of the biharmonic equation (equation 6) can be expressed in terms of two analytic functions $\phi(z)$ and $\chi(z)$ of the complex variable $z = x + iy$ or

$$U(x,y) = \mathrm{Re}[\bar{z}\phi(z) + \chi(z)], \tag{7}$$

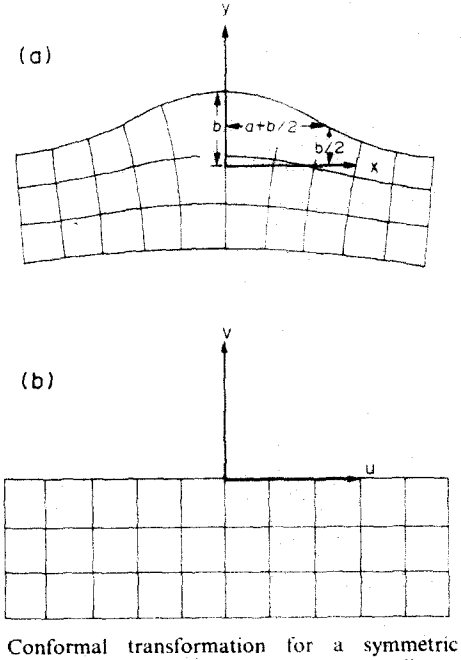

Fig. 1. Conformal transformation for a symmetric ridge in x,y-co-ordinates into a half-plane in u,v-co-ordinates and the definition of the parameters a and b which describe the shape of the ridge.

where Re indicates the real part of $\bar{z}\phi(z)+\chi(z)$ and $\bar{z}=x-iy$. Equation (7) can also be written as

$$2U(x,y)=\bar{z}\phi(z)+z\overline{\phi(z)}+\chi(z)+\overline{\chi(z)}, \quad (8)$$

where conjugate complex values are denoted by overbars. Differentiating equation (8) with respect to x and y and using equations (5a) (b) and (c) yields

$$\sigma_x+\sigma_y=4\,\mathrm{Re}[\Phi(z)]+\frac{\rho g y}{1-\mu}, \quad (9)$$

where $\Phi(z)=\phi'(z)$ and similarly

$$\sigma_y-\sigma_x+2i\sigma_{xy}=2[\bar{z}\Phi'(z)+\Psi(z)]+\left[\frac{1-2\mu}{1-\mu}\right]\rho g y, \quad (10)$$

where $\Psi(z)=\chi''(z)$. Details of the derivation of equations (9) and (10) are found in Muskhelishvili [15] and Sokolnikoff [16].

There are now expressions for the three stress components σ_x, σ_y and σ_{xy} in terms of two, as yet unknown, analytic functions of a complex variable $\Phi(z)$ and $\Psi(z)$. Before proceeding to the determination of these unknown functions for the case of a symmetric ridge or valley, the conformal mapping technique used to transform the ridge or valley into the lower half-plane and the transformation of the stress equations needed to find a closed solution are introduced.

The preceding theory is appropriate for orthogonal Cartesian co-ordinate systems with straight boundaries. For curvilinear boundaries, orthogonal curvilinear co-ordinate systems are introduced by a transformation $z=f(w)$ where $z=x+iy$ is a function of $w=u+iv$. Such a transformation that connects a point $P(x+iy)$ in the z-plane to a point $P'(u+iv)$ in the w-plane is conformal if angles between intersecting co-ordinate curves in the two systems are preserved. The conformal transformation for a symmetric ridge into a half-plane is given by

$$z=f(w)=w+\frac{ab}{w-ia}, \quad (11a)$$

or separated into real and imaginary parts by,

$$x=u+\frac{abu}{u^2+(v-a)^2}, \quad (11b)$$

$$y=v-\frac{ab(v-a)}{u^2+(v-a)^2}. \quad (11c)$$

Here, b represents the ridge height. When $u=a$ and $v=0$, then $x=a+b/2$ and $y=b/2$, which are the co-ordinates of the inflection point on the ridge flank. The slope at this inflection point is given by $dy/dx=-b/2a$. These relations and the conformal transformation are shown in Fig. 1. The transformation for a symmetric valley is obtained by changing the sign of b in equations (11). Note that for a valley, the parameter a must be greater than the absolute value of b otherwise a cusp is formed and transformation (11) will no longer be conformal.

Because of the property that analytic functions remain analytic under conformal transformation [17] the region of interest can, in principle, be carried into the lower half-plane where a solution can be found. Under this transformation equations (9) and (10) become [7 and 15, pp. 381–383]

$$\sigma_x+\sigma_y=4\,\mathrm{Re}[\Phi(w)]+\frac{1}{1-\mu}\rho g\,\mathrm{Im}f(w), \quad (12)$$

and

$$\sigma_y-\sigma_x+2i\sigma_{xy}=2\left[\frac{\overline{f(w)}}{f'(w)}\Phi'(w)+\Psi(w)\right]+\left[\frac{1-2\mu}{1-\mu}\right]\rho g\,\mathrm{Im}f(w), \quad (13)$$

where Im denotes the imaginary part of $f(w)$, that is, $y=\mathrm{Im}f(w)$.

Boundary conditions on $v=0$ of the w-plane are derived from the identity

$$\mathrm{N}+i\mathrm{T}=\frac{\sigma_u+\sigma_v}{2}+\frac{\sigma_v-\sigma_u+2i\sigma_{uv}}{2}, \quad (14)$$

where N and T represent applied normal and shear tractions. The boundary of the symmetric ridge or valley in the z-plane corresponds to the axis $v=0$ in the w-plane (Fig. 1). Because the boundary of the symmetric ridge or valley is free of load, $\mathrm{N}+i\mathrm{T}=0$ and

$$2\,\mathrm{Re}\Phi(u)+\frac{\overline{f(u)}}{\overline{f'(u)}}\Phi'(u)+\frac{f'(u)}{\overline{f'(u)}}\Psi(u)=-\frac{1}{2}\left[\frac{1}{1-\mu}\right]\rho g\,\mathrm{Im}f(u)-\frac{1}{2}\left[\frac{1-2\mu}{1-\mu}\right]\rho g\,\mathrm{Im}f(u)\frac{f'(u)}{\overline{f'(u)}}. \quad (15)$$

Denoting the right-hand side of equation (15) by $\mathrm{N}_{we}+i\mathrm{T}_{we}$ and multiplying through by $\overline{f'(u)}$ gives

$$\overline{f'(u)}\,\Phi(u)+\overline{f'(u)}\,\overline{\Phi(u)}+\overline{f(u)}\,\Phi'(u)+f'(u)\,\Psi(u)=\overline{f'(u)}\,[\mathrm{N}_{we}+i\mathrm{T}_{we}]. \quad (16)$$

The conjugate complex form of equation (16) is

$$f'(u)\,\overline{\Phi(u)}+f'(u)\,\Phi'(u)+f(u)\,\overline{\Phi'(u)}+\overline{f'(u)}\,\Psi(u)=f'(u)\,[\mathrm{N}_{we}-i\mathrm{T}_{we}]. \quad (17)$$

By using certain properties of Cauchy integrals [15] and equations (15) and (16), the unknown stress functions $\Phi(w)$ and $\Psi(w)$ are determined and hence the gravity-induced stresses in the symmetric ridge or valley by equations (12) and (13). Consider the terms on the left-hand side of equation (16). The term $\overline{f'(u)}\,\Phi(u)$ is the boundary value of

$$\left[\frac{(w+ia)^2-ab}{(w+ia)^2}\right]\Phi(w)$$

assumed to be analytic in the lower half-plane except

when $w = -ia$. The term $\overline{f'(u)}\,\overline{\Phi(u)}$ is the boundary value of

$$\left[\frac{(w+ia)^2 - ab}{(w+ia)^2}\right]\bar{\Phi}(w)$$

assumed analytic in the upper half-plane. Note that the partial overbar on a complex function $F(w)$ has a special meaning; that is [15], $\bar{F}(w) = \overline{F(\bar{w})}$. The next term, $\overline{f(u)}\,\Phi'(u)$, is the boundary value of

$$\left[w + \frac{ab}{w+ia}\right]\Phi'(w)$$

assumed analytic in the lower half-plane except at $w = -ia$ and the last term on the left-hand side of equation (16) is the boundary value of

$$\left[\frac{(w-ia)^2 - ab}{(w-ia)^2}\right]\Psi(w)$$

assumed to be analytic in the lower half-plane.

For equation (17) the term on the left-hand side is the boundary value of

$$\left[\frac{(w-ia)^2 - ab}{(w-ia)^2}\right]\bar{\Phi}(w)$$

assumed analytic in the upper half-plane except at $w = ia$, and the second term is the boundary value of

$$\left[\frac{(w-ia)^2 - ab}{(w-ia)^2}\right]\Phi(w)$$

assumed to be analytic in the lower half-plane. The term $f(u)\,\overline{\Phi'(u)}$ is the boundary value of

$$\left[w + \frac{ab}{w-ia}\right]\bar{\Phi}'(w)$$

assumed analytic in the upper half-plane except at $w = ia$ and the last term on the left-hand side of equation (17) is the boundary value

$$\left[\frac{(w+ia)^2 - ab}{(w+ia)^2}\right]\bar{\Psi}(w)$$

assumed to be analytic in the upper half-plane.

Some useful formulae obtained from the properties of Cauchy integrals are given by Muskhelishvili [15, pp. 269–272]. If a function $F(w)$ is analytic in the upper half-plane with the possible exception of a finite number of points where it may have poles with the principal parts $G_1(w), G_2(w), \ldots, G_n(w)$ then

$$\frac{1}{2\pi i}\int_{-\infty}^{\infty}\frac{F(u)\,du}{u-w} = F(w) - G_1(w) - G_2(w) - \ldots - G_n(w), \quad (18a)$$

for w in the upper half-plane and

$$\frac{1}{2\pi i}\int_{-\infty}^{\infty}\frac{F(u)\,du}{u-w} = -G_1(w) - G_2(w) - \ldots - G_n(w), \quad (18b)$$

for w in the lower half-plane. If $F(w)$ is analytic in the lower half-plane with the possible exception of a finite number of points where it may have poles with the principal parts $G_1(w), G_2(w), \ldots, G_n(w)$ then

$$\frac{1}{2\pi i}\int_{-\infty}^{\infty}\frac{F(u)\,du}{u-w} = -F(w) + G_1(w) + G_2(w) + \ldots + G_n(w), \quad (19a)$$

for w in the lower half-plane and

$$\frac{1}{2\pi i}\int_{-\infty}^{\infty}\frac{F(u)\,du}{u-w} = G_1(w) + G_2(w) + \ldots + G_n(w), \quad (19b)$$

for w in the upper half-plane.

Now introduce the following expansion about the poles at $w = \pm ia$. Let

$$\frac{\Phi(w)}{(w+ia)^2} = \Omega_0(w) + \frac{A_{-1}}{(w+ia)} + \frac{A_{-2}}{(w+ia)^2}, \quad (20a)$$

where the function $\Omega_0(w)$ is assumed analytic in the lower half-plane and A_{-1} and A_{-2} are complex constants. Expansion (20a) is then analytic in the lower half-plane except at $w = -ia$ and

$$\frac{\bar{\Phi}(w)}{(w-ia)^2} = \bar{\Omega}_0(w) + \frac{\bar{A}_{-1}}{(w-ia)} + \frac{\bar{A}_{-2}}{(w-ia)^2}, \quad (20b)$$

is analytic in the upper half-plane except at $w = ia$. Also let

$$\frac{\Phi'(w)}{(w+ia)} = \chi_0(w) + \frac{B_{-1}}{(w+ia)}, \quad (21a)$$

where the function $\chi_0(w)$ is assumed analytic in the lower half-plane and B_{-1} is a complex constant. Then expansion (21a) is analytic in the lower half-plane except at $w = -ia$ and

$$\frac{\bar{\Phi}'(w)}{(w-ia)} = \bar{\chi}_0(w) + \frac{\bar{B}_{-1}}{(w-ia)}, \quad (21b)$$

is analytic in the upper half-plane except at $w = ia$.

Applying the formulae (18) and (19) to equation (16) and using expansions (20a) and (21a), it is found that

$$f'(w)\,\Psi(w) = -B(w) - \Phi(w) - w\Phi'(w) + \frac{ab\Phi(w)}{(w+ia)^2} - \frac{ab\Phi'(w)}{(w+ia)} - \frac{ab[A_{-1} - B_{-1}]}{(w+ia)} - \frac{abA_{-2}}{(w+ia)^2}, \quad (22)$$

where

$$B(w) = \frac{1}{2\pi i}\int_{-\infty}^{\infty}\frac{\overline{f'(u)}\,[N_{we} + iT_{we}]\,du}{u-w}. \quad (23)$$

Similarly, applying formulae (18) and (19) to equation (17) and using expansions (20b) and (21b) it is found that

$$f'(w)\Phi(w) = -A(w) + \frac{ab[\bar{A}_{-1} - \bar{B}_{-1}]}{(w-ia)} + \frac{ab\bar{A}_{-2}}{(w-ia)^2}, \quad (24)$$

where

$$A(W) = \frac{1}{2\pi i}\int_{-\infty}^{\infty}\frac{f'(u)[N_{we} - iT_{we}]\,du}{u-w}. \quad (25)$$

To find the complex constants A_{-1}, B_{-1} and A_{-2} consider

the first three terms of a Taylor's series expansion of $\Phi(w)$ about $w = -ia$, or

$$\Phi(w) = \Phi(-ia) + \Phi'(-ia)(w + ia) + \frac{\Phi''(-ia)(w + ia)^2}{2}. \quad (26)$$

Then

$$\Phi'(w) = \Phi'(-ia) + \Phi''(-ia)(w + ia). \quad (27)$$

Dividing both sides of expansion (26) by $(w + ia)^2$ and comparing coefficients of like powers of $(w + ia)$ between expansions (20a) and (26) gives $A_{-1} = \Phi'(-ia)$ and $A_{-2} = \Phi(-ia)$. Dividing both sides of equation (27) by $w + ia$ and comparing coefficients of like powers of $w + ia$ between expansions (21a) and (27) gives $B_{-1} = \Phi'(ia) = A_{-1}$. Thus, equations (22) and (23) become

$$f'(w)\Psi(w) = -B(w) - \Phi(w) - \left[w + \frac{ab}{w + ia}\right]\Phi'(w) + \frac{ab[\Phi(w) - \Phi(-ia)]}{(w + ia)^2}, \quad (28)$$

and

$$f'(w)\Phi(w) = -A(w) + \frac{ab\Phi(-ia)}{(w - ia)^2}. \quad (29)$$

Since

$$f'(w) = 1 - \frac{ab}{(w - ia)^2}$$

equation (29) can be written as

$$\Phi(w) - \frac{ab\Phi(w)}{(w - ia)^2} = -A(w) + \frac{ab\bar{\Phi}(-ia)}{(w - ia)^2},$$

which becomes

$$4a\Phi(-ia) + b[\Phi(-ia) + \bar{\Phi}(-ia)] = -4aA(-ia),$$

at $w = -ia$. Let $\Phi(-ia) = \alpha + i\beta$

$$4a[\alpha + i\beta] + 2b\alpha = 4aA(-ia), \quad (30)$$

and $\Phi(-ia)$ can be found the real and imaginary parts of $A(-ia)$ which will be determined below.

Equation (11a), the right-hand side of equation (15) and equations (23) and (25) yield

$$A(w) = \frac{-\rho g a^2 b}{2(1 - \mu)}\left[\frac{i[4a + b]}{8a^2(w - ia)} + ab\left(\frac{1}{4a^2(w - ia)^2} - \frac{i}{2a(w - ia)^3}\right) + (1 - 2\mu)\left(\frac{i[4a + b]}{8a^2(w - ia)}\right)\right], \quad (31)$$

and

$$B(w) = \frac{-\rho g a^2 b}{2(1 - \mu)}\left\{\frac{i[4a + b]}{8a^2(w - ia)} + (1 - 2\mu)\left[\frac{i(4a + b)}{8a^2(w - ia)} + ab\left(\frac{1}{4a^2(w - ia)^2} - \frac{i}{2a(w - ia)^3}\right)\right]\right\}. \quad (32)$$

From equation (31) it is found that

$$A(-ia) = \rho g b\left[\frac{(4a + b)(1 - \mu) + b}{16a(1 - \mu)}\right],$$

which is real. Thus, β in equation (30) vanishes, and hence

$$\Phi(-ia) = \bar{\Phi}(-ia) = -\rho g b\left[\frac{(4a + b)(1 - \mu) + b}{8(1 - \mu)(2a + b)}\right]. \quad (33)$$

Dividing equations (28) and (29) by $f'(w)$ yields, finally, expressions for $\Psi(w)$ and $\Phi(w)$ from which stresses in the symmetric ridge or valley can be obtained through equations (12) and (13). These expressions are

$$\Psi(w) = \frac{-(w - ia)^2}{(w - ia)^2 - ab}\left\{B(w) + \Phi(w) + \left[w + \frac{ab}{w + ia}\right]\Phi'(w) - ab\frac{[\Phi(w) - \Phi(-ia)]}{(w + ia)^2}\right\}, \quad (34)$$

and

$$\Phi(w) = \frac{(w - ia)^2}{(w - ia)^2 - ab}\left\{A(w) - \frac{ab\Phi(-ia)}{(w - ia)^2}\right\}. \quad (35)$$

The derivative of $\Phi(w)$ with respect to w in equation (34) is

$$\Phi'(w) = \frac{-\rho g b}{8[(w - ia)^2 - ab]}\left\{i[4a + b] + \frac{2ab}{(1 - \mu)(w - ia)} - \frac{6ia^2 b}{(1 - \mu)(w - ia)^2}\right\} - \frac{2ab[\Phi(w) + \Phi(-ia)]}{(w - ia)[(w - ia)^2 - ab]}. \quad (36)$$

A singularity apparently occurs in equation (34) when $w = -ia$. However, substituting expansions (26) and (27) into equation (34) and evaluating the resulting expressions at $w = -ia$ one finds that $\Psi(w)$ is continuous; that is,

$$\Psi(-ia) = \frac{-4a}{4a + b} \times \left\{B(-ia) + \Phi(-ia) - ia\Phi(-ia) + \frac{ab\Phi''(-ia)}{2}\right\}, \quad (37)$$

where $\Phi''(-ia)$ derived from equation (36) is given by

$$\Phi''(-ia) = \frac{1}{a(4a + b)} \times \left[2\Phi(-ia) - 8ia\Phi'(-ia) + \frac{\rho g b^2}{16a(1 - \mu)}\right]. \quad [38]$$

To obtain the gravity-induced stresses in the symmetric ridge or valley one has from equations (12) and (35)

$$\sigma_x + \sigma_y = -4\mathrm{Re}\left\{\frac{(w - ia)^2}{(w - ia)^2 - ab} \times \left[A(w) - \frac{ab\Phi(-ia)}{(w - ia)^2}\right]\right\} + \frac{1}{1 - \mu}\rho g y, \quad (39)$$

and from equations (11a), (13), (34) and (36)

$$\sigma_y - \sigma_x + 2i\sigma_{xy} = \frac{2(w-ia)^2}{(w-ia)^2 - ab}\left\{\frac{[\bar{w}(\bar{w}+ia)+ab]}{\bar{w}+ia}\right.$$
$$\times \Phi'(w) - B(w) - \Phi(w)$$
$$-\left[w + \frac{ab}{w+ia}\right]\Phi'(w)$$
$$\left.+\frac{ab[\Phi(w)-\Phi(-ia)]}{(w+ia)^2}\right\}$$
$$+\left[\frac{1-2\mu}{1-\mu}\right]\rho g y. \qquad (40)$$

Expressions for $\sigma_y - \sigma_x$ and σ_{xy} are obtained by taking the real and imaginary parts of equation (40). As this can be done readily in FORTRAN [19], no further detail is necessary here, except to note that values for σ_x and σ_y at each point in the ridge or valley can be obtained by forming sums and differences between $\sigma_x + \sigma_y$ given by equation (39) and $\sigma_y - \sigma_x$ given by the real part of equation (40). The expressions for the stresses satisfy the conditions of the problem: namely, the shear stresses on the ridge (valley) surface and the stresses normal to the ridge (valley) surface vanish; the shear stresses vanish on the axial plane of the ridge (valley), and the stresses approach a standard stress state (equations 5a, b and c) away from the topographic feature.

EXAMPLES

Contour diagrams of dimensionless stresses $\sigma_x/\rho gb$, $\sigma_y/\rho gb$ and $\sigma_{xy}/\rho gb$ obtained from equations (39) and (40) for three symmetric ridges and three symmetric valleys are shown in Figs 2–7. Because of symmetry, only the right half of each feature is presented. Note that the signs of $\sigma_{xy}/\rho gb$ will be opposite on the left-hand halves. Figures 2–4 show three ridges for $a/b = 0.5$, 1 and 3.333, respectively and Poisson's ratio of 1/4. For the steepest hill, $a/b = 0.5$ (Fig. 2), note that $\sigma_x/\rho gb$ and $\sigma_{xy}/\rho gb$ are concentrated on the lower side of the ridge. As the ridges broaden and their slopes ($b/2a$) decrease, the concentrations of stresses diminish somewhat for $a/b = 1$ (Fig. 3) and vanish for $a/b = 3.333$ (Fig. 4). Also, with decreasing surface slope the contours of $\sigma_x/\rho gb$ and $\sigma_y/\rho gb$ become smoother and more nearly follow the ridge shapes.

Figures 5–7 show three valleys for $a/b = -1.1$, -2 and -3, respectively and Poisson's ratio of 1/3. For the narrowest valley, $a/b = -1.1$ (Fig. 5), there is a concentration of tensile $\sigma_x/\rho gb$ at the valley bottom, enclosed by the zero contour of $\sigma_x/\rho gb$ and a concentration of $\sigma_{xy}/\rho gb$ on the lower flanks of the valley. As the valleys broaden, the region of tensile $\sigma_x/\rho gb$ increases and two regions develop where $\sigma_{xy}/\rho gb$ is concentrated; one near the valley bottom and the other at greater depth and away from the valley bottom. Signs for these two concentrations are different as they lie on opposite sides of the zero shear-stress contour. For $a/b = -3$ (Fig. 7) the region over which $\sigma_x/\rho gb$ is tensile is again larger, as are the two regions where shear stresses of opposite sign are concentrated. Finally, in each of the latter two cases, contours of $\sigma_y/\rho gb$ follow the valley shape.

Figure 8a shows the orientations of principal stresses σ_1 and σ_3 in a symmetric ridge ($a/b = 1$; $\mu = 1/4$). Using engineering convention, the most compressive principal stress is σ_3 and the least compressive principal stress is σ_1. Note that the principal stress trajectories formed by curves that are everywhere tangent to the principal stress directions are of the interlocking type just below the ridge crest (Fig. 8a). Thus, on the centreline of the ridge there will be an isotropic point where $\sigma_1 = \sigma_3$.

Orientations of principal stresses for a valley ($a/b = -2$; $\mu = 1/4$) are shown in Fig. 8b. There are no isotropic points in this case; hence, σ_3, the most compressive principal stress, is nowhere equal to σ_1.

Figures 9a–c show the variation of $\sigma_x/\rho gb$, $\sigma_z/\rho gb$ (the out-of-plane normal stress defined by equation 3), and $\sigma_y/\rho gb$ with y/b along the centreline of the ridge ($a/b = 1$) for different values of Poisson's ratio. The short, dashed lines in the figures represent the variation of the standard stresses for the case when $b = 0$; that is,

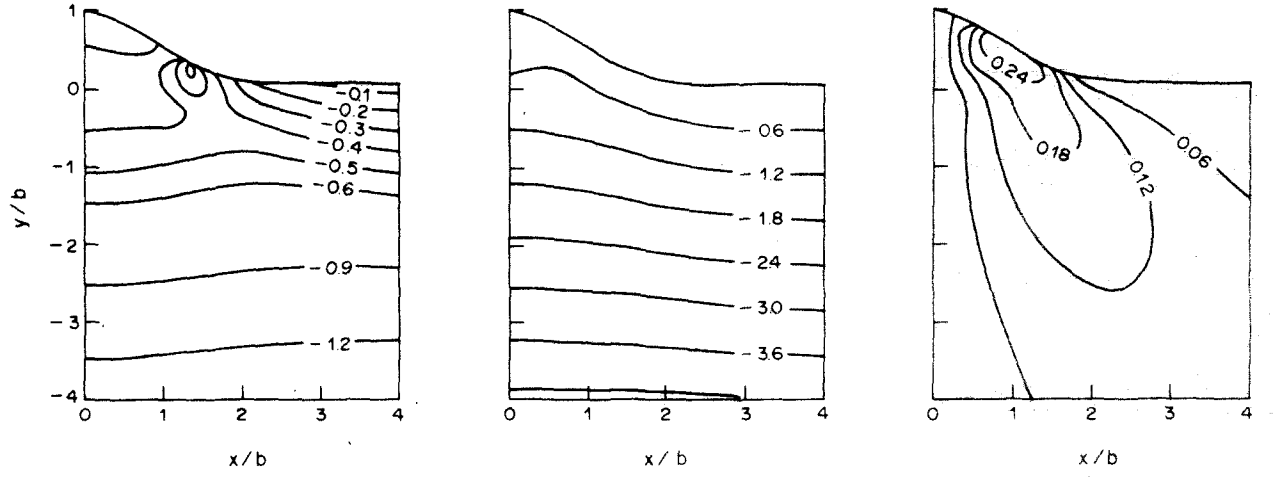

Fig. 2. Contour plots of $\sigma_x/\rho gb$, $\sigma_y/\rho gb$ and $\sigma_{xy}/\rho gb$ from left to right, respectively, for a symmetric ridge where $a/b = 0.5$ and $\mu = 1/4$.

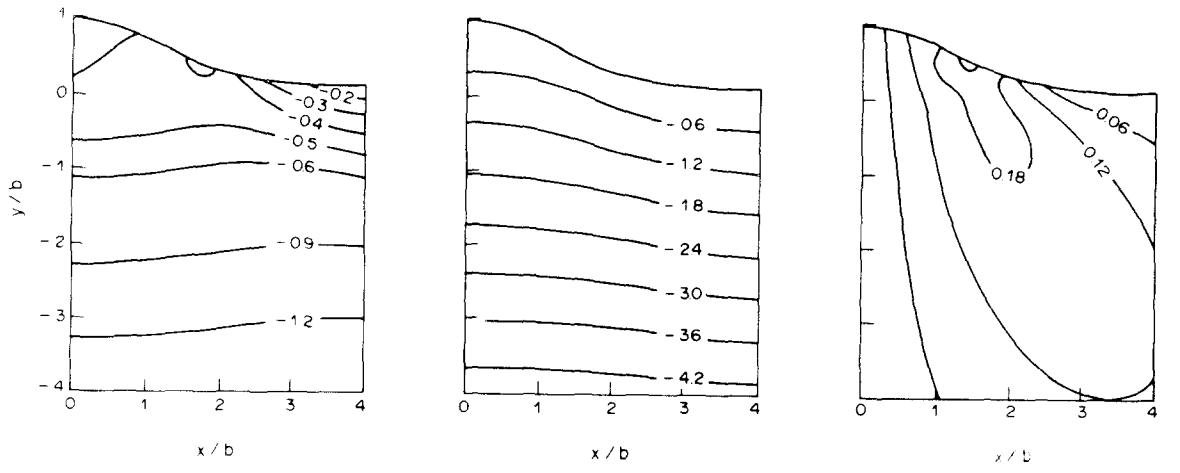

Fig. 3. Contour plots of $\sigma_x/\rho gb$, $\sigma_y/\rho gb$ and $\sigma_{xy}/\rho gb$ from left to right, respectively, for a symmetric ridge where $a/b = 1$ and $\mu = 1/4$.

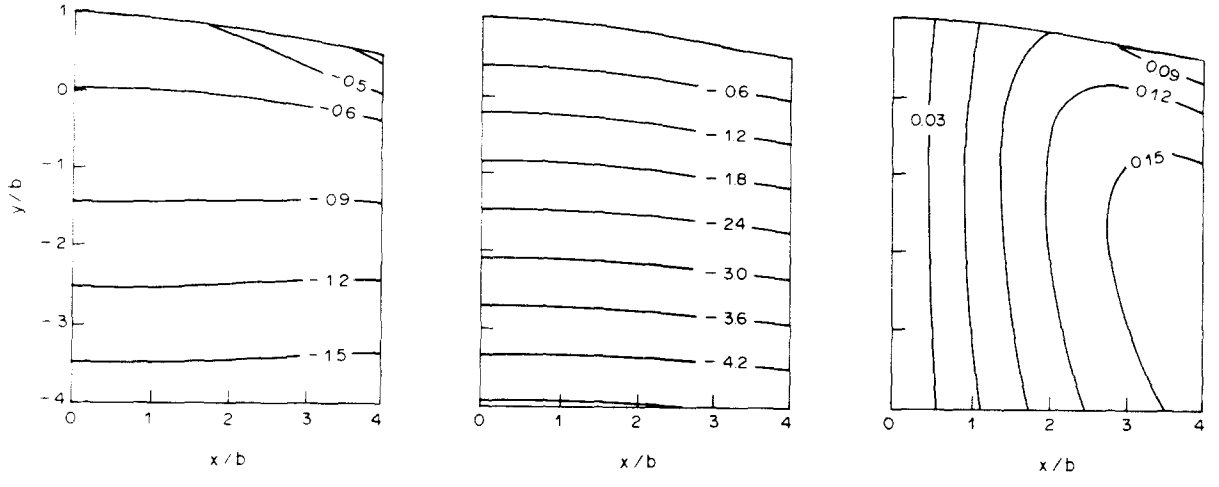

Fig. 4. Contour plots of $\sigma_x/\rho gb$, $\sigma_y/\rho gb$ and $\sigma_{xy}/\rho gb$ from left to right, respectively, for a symmetric ridge where $a/b = 3.333$ and $\mu = 1/4$.

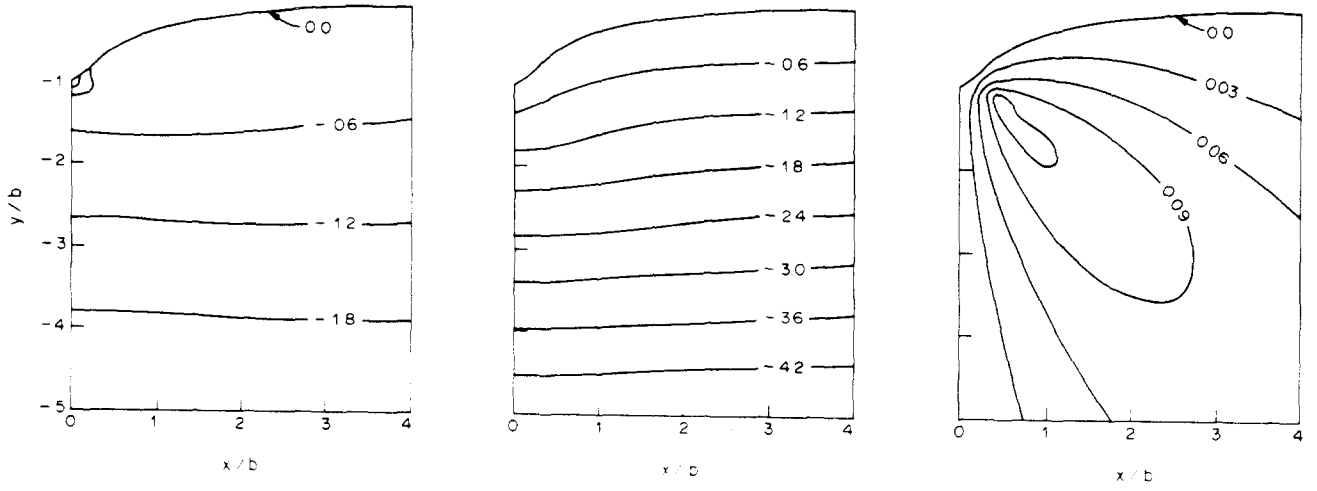

Fig. 5. Contour plots of $\sigma_x/\rho gb$, $\sigma_y/\rho gb$ and $\sigma_{xy}/\rho gb$ from left to right, respectively, for a symmetric valley where $a/b = -1.1$ and $\mu = 1/3$.

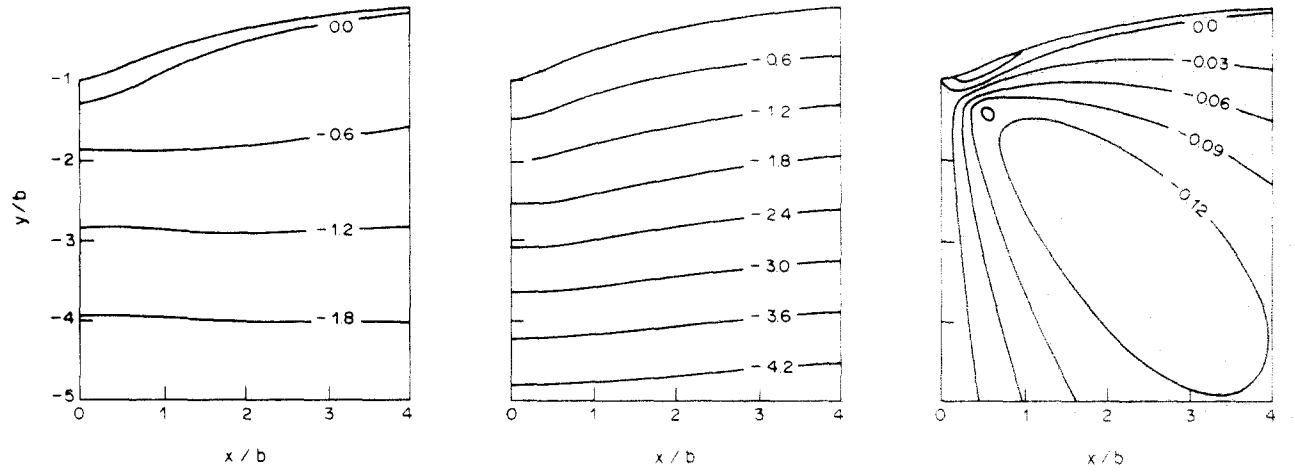

Fig. 6. Contour plots of $\sigma_x/\rho gb$, $\sigma_y/\rho gb$ and $\sigma_{xy}/\rho gb$ from left to right, respectively, for a symmetric valley where $a/b = -2$ and $\mu = 1/3$.

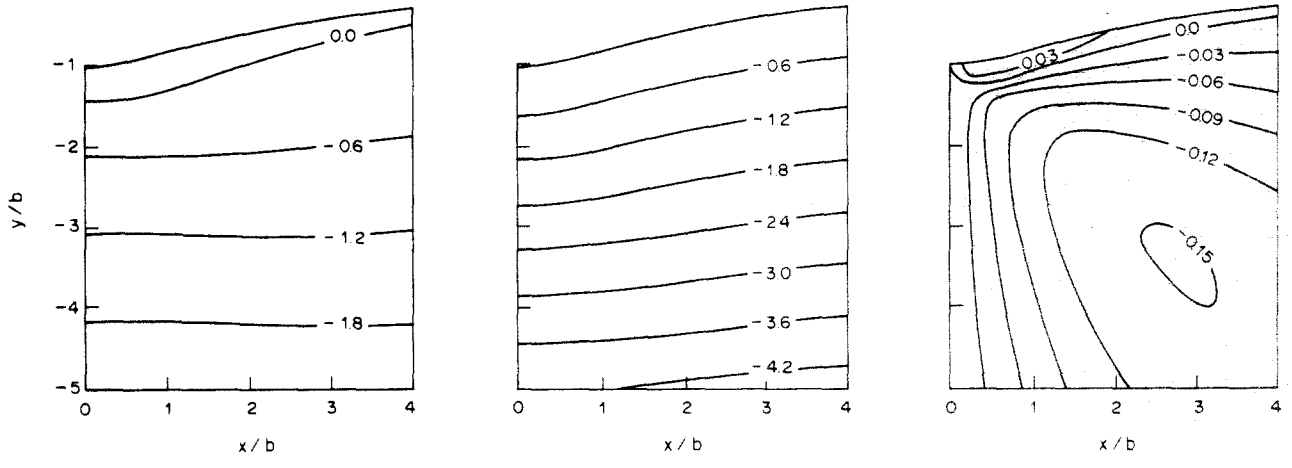

Fig. 7. Contour plots of $\sigma_x/\rho gb$, $\sigma_y/\rho gb$ and $\sigma_{xy}/\rho gb$ from left to right, respectively, for a symmetric valley where $a/b = -3$ and $\mu = 1/3$.

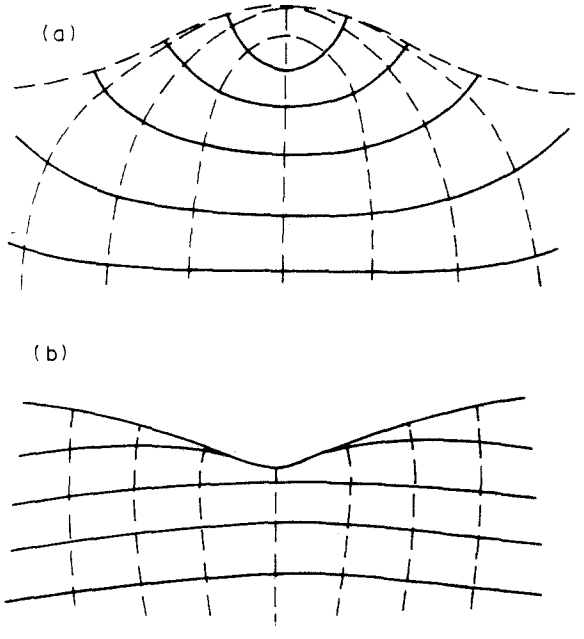

Fig. 8. Orientations of principal stresses in a symmetric ridge (a) where $a/b = 1$ and $\mu = 1/4$, and in a symmetric valley (b) where $a/b = -2$ and $\mu = 1/4$. The least compressive stress is σ_1 (solid line) and the greatest compressive stress is σ_3 (dashed line).

when there is no ridge. The topographically-induced stresses in the ridge become, with increasing depth, asymptotic to these standard stresses. As would be expected, a broader ridge affects the stress field to a greater depth. For example, the stress caused by the broad ridge ($a/b = 3$) is 1.5 times the far-field standard stress at a depth 3 times the ridge height; whereas, the stress caused by a narrow ridge ($a/b = 0.5$) is within 10% of the far-field standard stress at comparable depths. Increasing the Poisson's ratio, μ, causes a decrease of $\sigma_x/\rho gb$ at the ridge crest but an increase at greater depth. The dimensionless, out-of-plane stress, $\sigma_z/\rho gb$, is little affected by changes in μ at the ridge crest but increases with μ at depth. The effect of changes in μ on $\sigma_y/\rho gb$ is negligible for all depths. The depth at which the isotropic point occurs on the centreline of the ridge can be estimated by comparing Figs 9a and c; for $\mu = 1/4$ the isotropic point is approximately at $y/b = 0.6$.

Figures 10a–c show the variation of $\sigma_x/\rho gb$, $\sigma_z/\rho gb$ and $\sigma_y/\rho gb$ with y/b along the centreline of a valley ($a/b = -3$) for different values of Poisson's ratio. The short, dashed lines in these figures again indicate the variation of the standard stresses in the absence of a

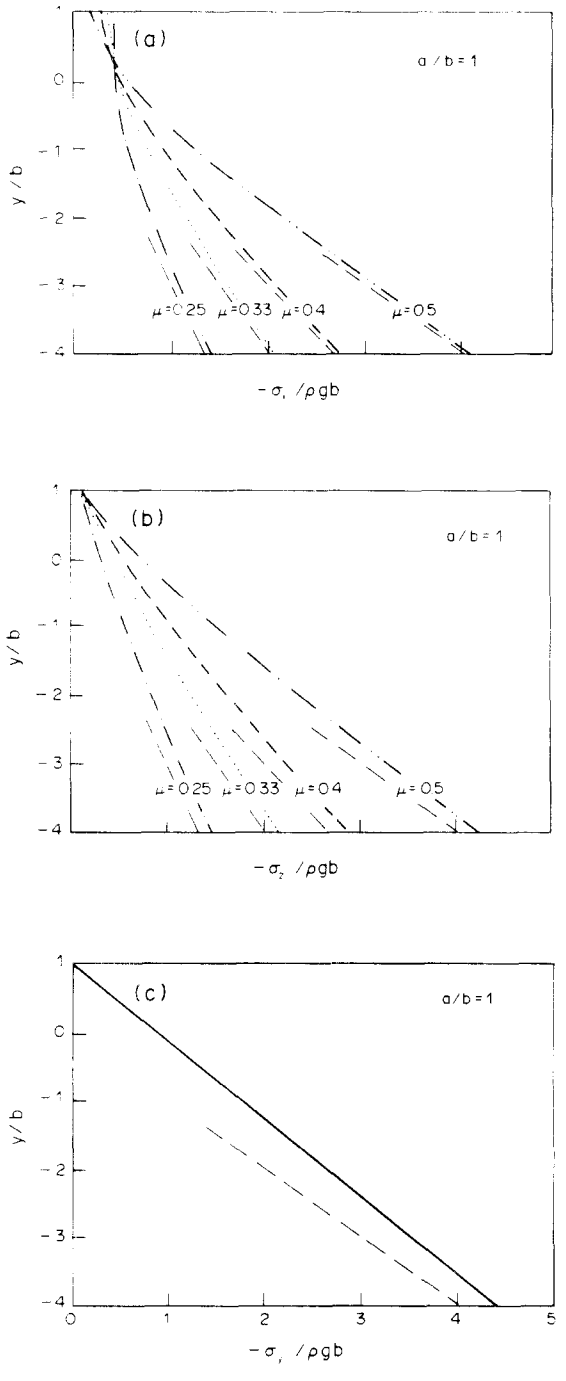

Fig. 9. Variation of $\sigma_x/\rho gb$ (a) and $\sigma_z/\rho gb$ (b) with y/b along the central plane of a symmetric ridge ($a/b = 1$) for four values of Poisson's ratio. The variation of $\sigma_y/\rho gb$ (c) with depth is little affected by changes in Poisson's ratio. The dashed lines indicate the change of the dimensionless stresses with depth in the absence of topography ($b = 0$).

valley ($b = 0$). As before, the stresses associated with the valley become, with increasing depth, asymptotic to the standard stresses. However, in valleys the gravitationally induced stresses approach the far-field standard stress rapidly for all values of a/b. This occurs because the valley, unlike the ridge, represents a deficiency in mass. As Poisson's ratio, μ, increases, the dimensionless stresses $\sigma_x/\rho gb$ and $\sigma_z/\rho gb$ become less tensile (more compressive) for all depths, while changes in μ have a negligible effect on $\sigma_y/\rho gb$.

COMPARISON WITH McTIGUE AND MEI'S APPROXIMATE SOLUTION FOR A SYMMETRIC RIDGE

McTigue and Mei [5] present approximate plane-strain elastic analytic solutions for the effect of topography with small slopes on gravity-induced stresses. Their solutions are based on a perturbation scheme which gives approximations of the dimensionless stress fields to an order ϵ^2, where ϵ is a characteristic slope. The slope ϵ is equal to H/L, where H is a characteristic height (equivalent to b in this paper) and L is a characteristic length of a topographic feature. Although several

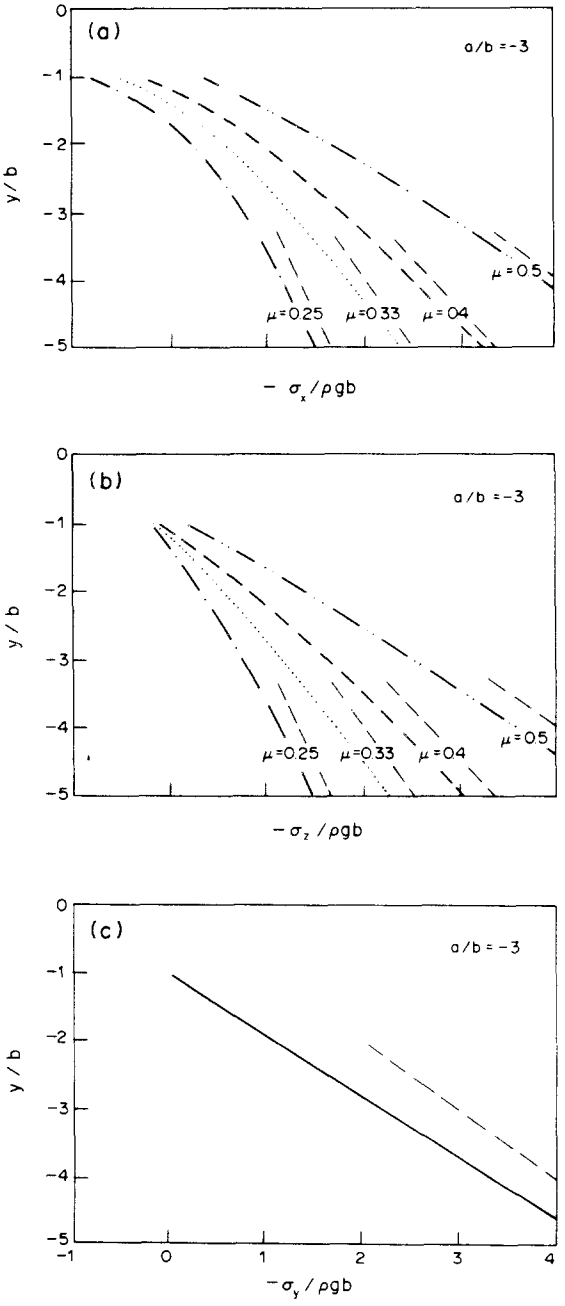

Fig. 10. Variation of $\sigma_x/\rho gb$ (a) and $\sigma_z/\rho gb$ (b) with y/b along the central plane of a symmetric valley ($a/b = -3$) for four values of Poisson's ratio. The variation of $\sigma_y/\rho gb$ (c) with depth is little affected by changes in Poisson's ratio. The dashed lines indicate the change of the dimensionless stresses with depth in the absence of topography ($b = 0$).

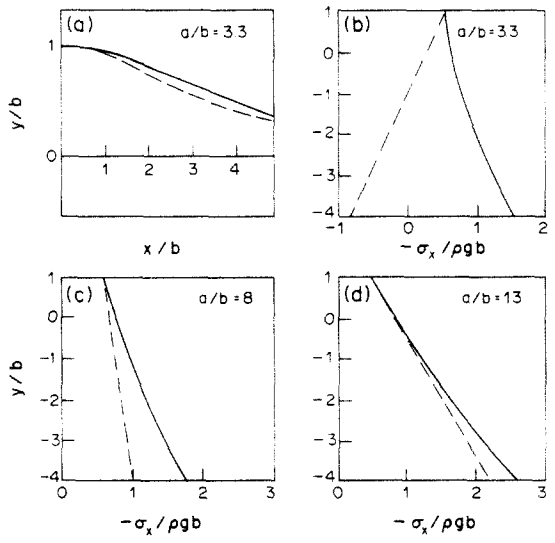

Fig. 11. Comparison of results obtained by the exact solution (solid line) and the approximate solution of McTigue and Mei [5] (dashed line). (a), Surface topography of the right half of a symmetric ridge for which $a/b = 3.3$; (b–d), dimensionless horizontal stress, $\sigma_x/\rho gb$, along the central planes of symmetric ridges whose parameters are $a/b = 3.3$, $\mu = 1/4$; $a/b = 8$, $\mu = 1/4$; and $a/b = 13$, $\mu = 1/3$.

different topographic features are discussed in their paper, only their approximate solution for an isolated, symmetric ridge is considered here. Expressions for surface topography and stresses in a symmetric ridge are given in terms of x/L, y/L and a parameter a which is called a' to distinguish it from the parameter a used in this paper. When the expressions of McTigue and Mei [5] are normalized by our b rather than L (for the purpose of comparing the two solutions) it is found that the two parameters, a and a', are related by $a' = \epsilon a$ and that $x/b = x/\epsilon L$. Figure 11a compares the surface topography (in terms of a and b) of the right half of the symmetric ridge from McTigue and Mei [5] (dashed line) with that given by equation (11c) (solid line) in this paper. As can be seen, the two surface topographies are reasonably similar.

Figures 11b–d show comparisons between $\sigma_x/\rho gb$ for the exact (solid lines) and approximate (dashed lines) solutions on the centreline of the symmetric ridge for $a/b = 3.3$, $\mu = 1/4$; $a/b = 8$, $\mu = 1/4$; and $a/b = 13$, $\mu = 1/3$, respectively. For the case $a/b = 3.3$, $\mu = 1/4$ (Fig. 11b) the value of $\sigma_x/\rho gb$ obtained by the approximate solution nearly matches the exact solution at the ridge crest, but becomes tensile with depth. The exact solution indicates no tension, rather the stress component asymptotically approaches the far-field standard stress state. For the case $a/b = 8$, $\mu = 1/4$ (Fig. 11c) both solutions predict that $\sigma_x/\rho gb$ remains compressive with depth, however, with the exception at the ridge crest, the comparison between the two solutions is still not good. It is of interest to note that for $a/b = 6$, $\mu = 1/4$ (a geometry intermediate to those shown in Figs 11b and c), the approximate solution predicts that the value of $\sigma_x/\rho gb$ remains constant at -0.583 for all depths. Finally, for the case $a/b = 13$, $\mu = 1/3$ (Fig. 11d) the two solutions give comparable results in the vicinity of the ridge. This case, however, represents a broad ridge with small surface slopes ($\tan^{-1}(b/2a) = 2.2°$).

Figure 12 shows contour plots of $\sigma_x/\rho gb$ and $\sigma_{xy}/\rho gb$ for a symmetric ridge ($a/b = 3.3$, $\mu = 1/4$) predicted by the approximate solution of McTigue and Mei [5]. These plots are identical to Figs 2a and c in their paper except that the solution is extended to greater depth and the horizontal scale is in terms of x/b rather than x/L. These contour plots of stresses can be compared with those for the exact solution shown in Fig. 4 of this paper. Again the comparison is poor in terms of the distribution, magnitude and sign of the stress components.

DISCUSSION

The ideas and results presented here are an outgrowth of an interest in measurement and analysis of stress fields in the near surface of the earth. It is envisioned that near-surface stress fields are primarily composed of gravitational stresses, thermal stresses and tectonic

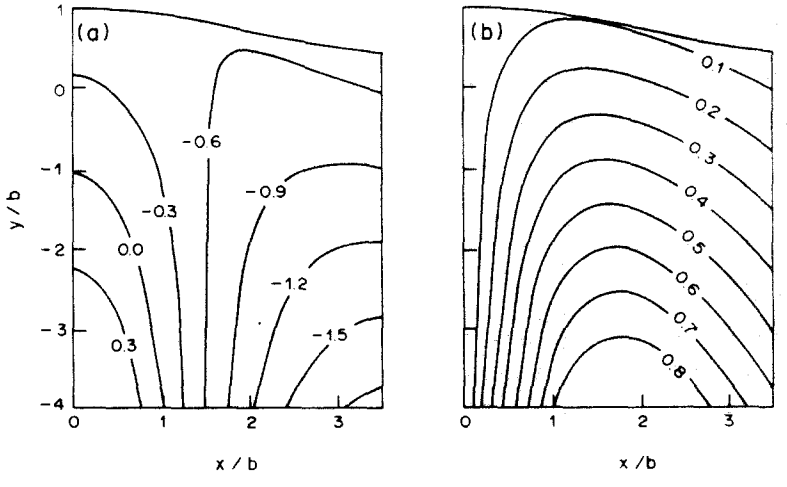

Fig. 12. Contour plots of $\sigma_x/\rho gb$ (a) and $\sigma_{xy}/\rho gb$ (b) for a symmetric ridge ($a/b = 3.3$, $\mu = 1/4$) computed by the perturbation method of McTigue and Mei [5].

stresses. Analyses of the topographic modification of a far-field tectonic compression or tension are given in Jaeger and Cook [18, p. 361], and by Harrison [20], McTigue and Mei [5], and McTigue and Stein [21]. Presently, we are developing our own analysis of this effect on the near-surface stress fields and will publish the results separately. Thermal stresses result from the passage of annual temperature waves from the surface downward, and from the geothermal gradient. Measurement and analyses of these stresses are given in Hooker and Duvall [22], Harrison and Herbst [23], Berger [24], Sbar *et al.* [25] and Swolfs and Savage [26]. The influence of topography on gravitational stresses in two particular cases is the subject of this paper, in which the mathematics broadly outlined by Akhpatelov and co-workers is derived in detail.

Interest in the topographic modification of gravitational stresses was originally directed towards the work of McTigue and Mei [5]. However, after carefully considering the implications of their analysis, it seemed physically implausible to have tension develop in symmetric ridges of small to moderate slope under the action of gravity alone. This led to the available Russian literature which, as mentioned earlier, was incomplete and not always explicit. Moreover, as presented, the solutions were quite complicated and, in fact, characterized as cumbersome by Ter-Martirosyan *et al.* [13]. This is, indeed, true when the solutions are separated into real and imaginary parts [12]. However, if the expressions are left in complex form as in equations (39) and (40), then $\sigma_x/\rho gb$, $\sigma_y/\rho gb$ and $\sigma_{xy}/\rho gb$ can be directly obtained using a FORTRAN program [19] that greatly reduces the algebraic and computational efforts.

The results obtained from equations (39) and (40) should give reasonable estimates of the stresses in isolated symmetric ridges and valleys provided that the earth materials making up these features behave elastically (or nearly so), excavation or accretion of these earth materials is not occurring [27], thermal effects are accounted for and tectonic stresses are absent or can be independently estimated. Of particular note is that, even for isolated symmetric ridges of low surface slope (Fig. 11), there persist non-zero compressive horizontal stresses near the crest of the features. Such stresses have indeed been measured [1], but interpreted in various ways as tectonic, residual, or otherwise, because it was generally believed that corrections from the topographic effect would be small. Of importance also is the prediction of tensile stresses in valley bottoms for typical laboratory values of Poisson's ratio. One would suspect that such tensile stresses could not be maintained in rocks of low tensile strength, or, perhaps, Poisson's ratios are high enough to preclude the development of tensile stresses in valleys (see Fig. 10a).

Clearly, the effect of topography defined by equations (11a, b and c) on far-field tectonic stresses can be analyzed separately in the manner outlined in this paper. This would allow the independent estimate of tectonic stresses mentioned earlier, as well as an assessment of the near-surface stresses due to both a body force and a tectonic stress in the vicinity of a symmetric ridge or valley.

CONCLUSIONS

An analysis of the topographic modification of the gravitationally induced stresses using an elastic solution similar to one originally given by Akhpatelov and co-workers [12–14] has been presented. The results, as stated here in equations (39) and (40), explicitly yield estimates of the stresses in the vicinity of isolated symmetric ridges and valleys. The magnitude of these stresses are of the order of the characteristic stress, ρgb, where b is the height of the ridge or the depth of the valley and vary with Poisson's ratio. Non-zero horizontal compressive stresses develop at or near ridge crests, persist even when surface slopes are small and decrease with increasing Poisson's ratio. Large horizontal tensile stresses develop under valleys, but decrease and become compressive with increasing Poisson's ratio. In the far field, all stresses approach the standard state of stress; that is, they are all compressive. The implications of this work are of importance and should aid in the solution of problems in regional geomechanics, tectonics and structural geology.

Received 4 *January* 1985; *revised* 26 *March* 1985.

REFERENCES

1. McGarr A. and Gay N. C. State of stress in the Earth's crust. *A. Rev. Earth Planet. Sci.* **6**, 405–436 (1978).
2. Haimson B. C. New hydrofracturing measurements in the Sierra Nevada Mountains and the relationship between shallow stresses and surface topography. *Proc. 20th U.S. Symp. on Rock Mechanics*, pp. 675–682. Austin (1979).
3. Swolfs H. S. The triangular stress diagram—a graphical representation of crustal stress measurements. *U.S. Geol. Surv. Prof. Paper* **1291**, 19 pp (1984).
4. Hooker V. E., Bickel D. L. and Aggson J. R. *In situ* determination of stresses in mountainous topography. *USBM RI* **7654**, 19 pp (1972).
5. McTigue D. F. and Mei C. C. Gravity-induced stresses near topography of small slope. *J. geophys. Res.* **86(B10)**, 9268–9278 (1981).
6. Tsytovich N. A. Problems of soil and rock mechanics in geomechanics. Special lecture. *Proc. VIII Int. Conf. on Soil Mechanics and Foundation Engineering*, Vol. IV, pp. 149–176. Moscow (1973).
7. Baladi G. Y. Distribution of stresses and displacements within and under long elastic and viscoelastic embankments, 175 pp. Ph.D. thesis, Purdue Univ., Indiana (1968).
8. Perloff W. H., Baladi G. Y. and Harr M. E. Stress distribution within and under long elastic embankments. *Highw. Res. Rec.* **181**, 12–40 (1967).
9. Cleary M. P. Fracture discontinuities and structural analysis in resource recovery endeavors. *J. Pressure Vessel Tech.* **100**, 2–12 (1978).
10. Silvestri V. and Tabib C. Exact determination of gravity stresses in finite elastic slopes—Part I. Theoretical considerations. *Can. Geotech. J.* **20**, 47–54 (1983).
11. Silvestri V. and Tabib C. Exact determination of gravity stresses in finite elastic slopes—Part II. Applications. *Can. Geotech. J.* **20**, 55–60 (1983).
12. Akhpatelov D. M. and Ter-Martirosyan Z. G. The stressed state of ponderable semi-infinite domains. *Armenian Acad. Sci. Mech. Bull.* **24(3)**, 33–40 (1971).
13. Ter-Martirosyan Z. G. and Akhpatelov D. M. The stressed state of an infinite slope with a curvilinear boundary object to a field of gravity and percolation. *J. Probl. Geomech.* **5**, 81–91 (1972).

14. Ter-Martirosyan Z. G., Akhpatelov D. M. and Manvelyan R. G. The stressed state of rock masses in a field of body forces. *Proc. 3rd Congr. ISRM*, Vol. 2 (Part A), pp. 569–574 (1974).
15. Muskhelishvili N. I. *Some Basic Problems of the Mathematical Theory of Elasticity*, 718 pp. Noordhoof, Groningen, The Netherlands (1953).
16. Sokolnikoff I. S. *Mathematical Theory of Elasticity*, 2nd edn, 476 pp. McGraw-Hill, New York (1956).
17. Kreyszig E. *Advanced Engineering Mathematics*, 898 pp. Wiley, New York (1967).
18. Jaeger J. C. and Cook N. G. W. *Fundamentals of Rock Mechanics*, 513 pp. Methuen, London (1969).
19. Savage W. Z., Powers P. S. and Swolfs H. S. RVT—a FORTRAN program for the exact solution for gravity and tectonic stresses in symmetric ridges and valleys. *U.S. Geol. Surv. Open-File Rept* **84-827**, 12 pp (1984).
20. Harrison J. C. Cavity and topographic effects in tilt and strain measurements. *J. geophys. Res.* **81(2)**, 319–328 (1976).
21. McTigue D. F. and Stein R. S. Topographic amplification of tectonic displacement—implications for geodetic measurements of strain changes. *J. geophys. Res.* **89(B2)**, 1123–1131 (1984).
22. Hooker V. E. and Duvall W. I. *In situ* rock temperature—stress investigations in rock quarries. *USBM RI* **7589**, 12 pp (1971).
23. Harrison J. C. and Herbst K. Thermoelastic strains and tilts revisited. *Geophys. Res. Lett.* **4(11)**, 535–537 (1977).
24. Berger J. A note on thermoelastic strains and tilts. *J. geophys. Res.* **80(2)**, 274–277 (1975).
25. Sbar M. L., Richardson R. M., Flaccus C. and Engelder T. Near-surface *in situ* stress, 1, Strain relaxation measurements along the San Andreas fault in southern California. *J. geophys. Res.* **89(B11)**, 9232–9332 (1984).
26. Swolfs H. S. and Savage W. Z. Site characterization studies of a volcanic cap rock. *Proc 25th U.S. Symp. on Rock Mechanics*, pp. 370–380. Evanston (1984).
27. Pariseau W. G. Influence of topography on the pre-mining state of stress. *Proc. 7th Canadian Symp. on Rock Mechanics*, pp. 191–200. Edmonton (1971).